Electronic Supplementary Information

Cation Distribution and Vacancies in Nickel Cobaltite

Danilo Loche[a], Claudia Marras[a], Daniela Carta[b] , Maria Francesca Casula[a], Gavin Mountjoy[c] and Anna Corrias[c]*

[a]*Dipartimento di Scienze Chimiche e Geologiche and INSTM, Università di Cagliari, I-09042 Monserrato, Cagliari, Italy.*

[b]*Department of Chemistry, University of Surrey, Guildford GU2 7XH.*

[c]*School of Physical Sciences, Ingram Building, University of Kent, Canterbury, CT2 7NH, UK.*

* **Corresponding Author**: a.corrias@kent.ac.uk

Aerogel Synthesis

Tetraethoxysilane ($Si(OC_2H_5)_4$, Aldrich 98%, TEOS), and cobalt (II) and nickel (II) nitrates ($Co(NO_3)_2 \cdot 6H_2O$ Aldrich 98% and $Ni(NO_3)_2 \cdot 6H_2O$ Aldrich 100%) were used as precursors for the silica matrix and for the cobaltite nanoparticles, respectively, and absolute ethanol (Fluka) was used as mutual solvent. The amounts of the precursors were chosen in such a way to obtain ~13 wt% of the desired $NiCo_2O_4$ phase in the final nanocomposite (mass of $NiCo_2O_4$ with respect to the total mass of the nanocomposite). This composition corresponds to an overall metal content of 10 wt% (mass of Co+Ni, in a 2:1 molar ratio, with respect to the total mass of the nanocomposite).

Briefly, the alcogel was obtained by pre-hydrolysis of TEOS and the metal salts under acidic catalysis, followed by the addition of urea (NH_2CONH_2, Sigma-Aldrich, >99.0%). The

latter is used to promote a fast and homogeneous gelation. After reflux for 35 minutes at 85 °C, a very viscous sol was obtained, which was poured into a closed container and allowed to gel at 40 °C. Gelation occurs in less than 12 hours with an extremely limited volume reduction. The corresponding aerogel was obtained by high temperature supercritical drying of the alcogel in an autoclave (Parr, 300 cm^3), which was filled with 70 mL of ethanol and flushed with N_2 before being closed and heated up to 330 °C. At this temperature the pressure in the autoclave reached 70 atm ensuring that the solvent was in the supercritical state. The autoclave was therefore vented down to atmospheric pressure, and the aerogel was obtained.

EXAFS and XANES data analysis

The program Viper was used to sum the data, identify the beginning of the absorption edge, E_0, fit pre and post edge backgrounds, and hence to obtain the normalised absorbance χ as a function of the modulus of the photoelectron wavevector k.[23] The modular package DL_EXCURV,[24] based on the EXCURV98 code, was used in the final stage of data processing to model the experimental $\chi(k)$ in order to extract structural information. This code uses fast curved wave theory and calculates ab initio the effective curved wave backscattering amplitude of the scatterer,[25] the phase shift due to the absorbing atom potential, the phase shift due to the scatterer, and the inelastic mean free path of the photoelectron.[26-27] The S_0 parameter (called AFAC in EXCURV98), which is the many-body amplitude reduction factor, was determined to be 0.9 from fitting to the reference samples. The parameter EF, which is a correction to E_0 was free to vary in all fittings. The structural parameters were obtained by non-linear least squares fitting in k-space with a k^3 weighting to emphasize the high-energy part of the spectrum. The fitting was carried out using the k range 2.5-12 $Å^{-1}$, at all edges. The errors in the fit parameters were obtained from the 95% confidence level, as calculated in EXCURV98. The number of fitted parameters was always

less than the number of statistically independent data points, as estimated in the standard way.[28] The quality of the fit was judged from the normalized sum of residuals

$$\text{R-factor} = \Sigma_n \, k_n^3 \, | \, \chi_{expt}(k_n) - \chi_{fit}(k_n) \, | \, / \, \Sigma_n \, k_n^3 \, | \, \chi_{expt}(k_n) \, | \times 100 \quad (1)$$

R-factors were calculated both on the experimental $k^3\chi(k)$ and on the data obtained by back transforming the Fourier transforms (FTs) in the region of R space corresponding to the shells which were fitted. The second value, named R*-factor, is more meaningful in stating the goodness of the fit since the backtransforms do not contain low R contributions due to imperfect background removal and high R contributions which were not included in the fitting. Reasonable EXAFS fits of single shells typically have values of R-factor around 20%; however, when the fit is performed on the total EXAFS spectra, higher values of R-factor can still correspond to good fits especially if the fit is not extended to peaks at high R.

The XANES spectra were processed in the usual way to obtain normalized absorbance.[29] XANES at the K-edge involves the excitation of a 1s photoelectron into low-lying empty states at the central atom with p-type symmetry. The characteristic features of the XANES spectra for transition metal oxides[30] are as follows. An increase in valence of the metal atom causes a shift to higher energies. Pre-edge peak(s) may occur at about 15-20 eV before the main K-edge corresponding to 1s to 3d transitions with 3d-4p mixing. The pre-edge peak increases in intensity as the degree of centrosymmetry of the metal atom environment decreases. The main peak and shoulders of the absorption edge corresponds to transitions to 4p continuum states and “shape resonances” of the metal atom environment. For a given environment, the main peak is broadened by disorder in the nearest neighbor distances. Secondary peaks occurring a few 10 eV above the main peak correspond to multiple scattering from neighboring atom shells.

The pre-edge peak has well-known behavior for sites with tetrahedral and octahedral symmetry (*i.e.* those present in spinels), being narrower and more intense for the former and broader and less intense for the latter. This is primarily because tetrahedral symmetry is highly non-centrosymmetric and this enables p-d mixing and thus 1s transitions to states with some d character which contribute to the pre-edge peak.[27] In addition, the shape of the pre-edge peak is influenced by the splitting of d-states which is different for tetrahedral and octahedral site symmetry.[31-32] The typical splitting is 1.5 eV, but this cannot be observed because the core-hole lifetime at transition metal K-edges is somewhat larger than 1 eV,[27] and the monochromator used in the present study had an energy resolution of 1.0 eV. When both tetrahedral and octahedral sites are occupied, the pre-edge peak will be the sum of these contributions, and will increase in intensity directly with the proportion of tetrahedral sites.[31,33]

The current qualitative analysis of the pre-edge peaks is based on the marked differences expected between tetrahedral and octahedral sites due to contributions from dipole transitions. It does not attempt assess different contributions from regular and distorted octahedral sites which would require detailed consideration of quadrupole transitions.[S1]

Ni:Co ratios

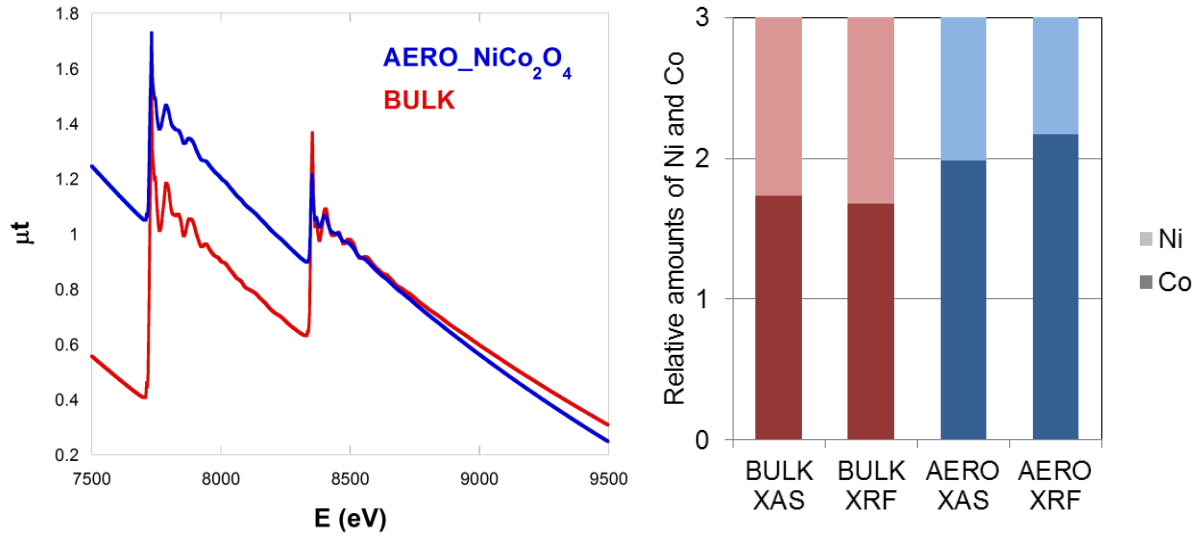

Figure S1. X-ray Absorption Spectra (left) and comparison between relative amount of Ni and Co as obtained by X-ray Absorption spectra and by XRF (right) for the AERO_$NiCo_2O_4$ and BULK samples.

Since the X-ray Absorption spectra at the Co and Ni K-edges were measured during a single scan it is possible to use the spectra to make a precise experimental determination of the Ni:Co ratio. (Note that this is a special case, and that X-ray absorption spectroscopy is not usually used to determine compositions because multiple elemental absorption edges are not usually measured in a single scan). In particular, the compilation of the X-ray absorption cross sections for the elements was used to determine with accuracy the expected ratio between the jumps at the Co and Ni K-edge on the basis of the nominal 1:2 Ni:Co composition of the BULK and AERO_$NiCo_2O_4$ samples. In the case of the AERO_$NiCo_2O_4$ sample the ratio of the jumps which were measured experimentally is very close to the theoretical value, which is 2.28, confirming that the cobaltite nanoparticles have a Ni:Co molar ratio very close to the nominal 1:2 value. Instead in the case of the BULK sample the ratio of the jumps which were measured experimentally is consistent with a Ni:Co molar ratio

equal to 1.2:1.8 indicating that some cobalt is lost during the synthesis which was carried out using a method taken from the literature.

The Ni:Co molar ratio was further investigated using a PANalytical Epsilon3 XRF spectrometer to obtain semi-quantitative results by using a "standard-less" measurement method. (In fact, due to the low amount of sample it was not possible to make fusion beads which are needed to obtain fully quantitative results by using a calibrated measurement method.) Nevertheless, the semi-quantitative XRF results confirm that the Ni:Co ratio is lower in the BULK sample, as shown in Figure S1.

XRD

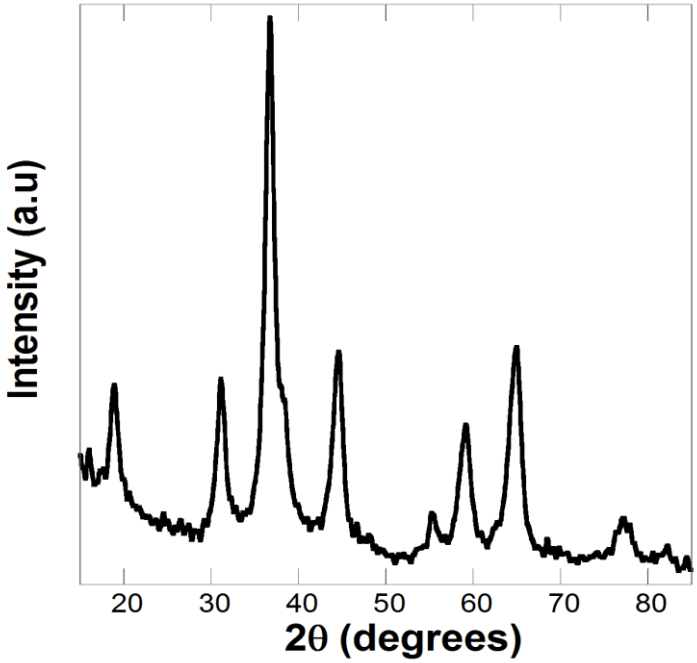

Figure S2. XRD pattern of the BULK sample.

N_2 physisorption at 77K

Surface areas, pore sizes and pore volumes of the AERO_$NiCo_2O_4$ sample were obtained from N_2 adsorption-desorption measurements at 77K recorded on a Sorptomatic 1990 System (Fisons Instrument). Prior to measurements, the samples were outgassed at 200

°C for 12 h. Surface area was estimated using the Brunauer-Emmett-Teller (BET) model[S2] and pore size and pore volumes were estimated using the Barret-Joyner-Halenda (BJH) method.[S3]

The isotherm, shown in Figure S3, can be classified as type IIb with an H3 hysteresis loop located at high values of relative pressures[S4] indicating the occurrence of interconnected mesopores with large size typical of the aerogel structure. In particular, the pore size is in the range 20-40 nm, the pore volume is 2.95 cm^3/g and the surface area is 448 m^2/g, values comparable to the ones observed in nanocomposites made out of ferrite nanoparticles dispersed in a highly porous silica aerogel matrix that is able to disperse the nanoparticles and protect them.[20-21] As also suggested by TEM investigation, the porous texture of the silica aerogel matrix enables a fine dispersion of the cobaltite nanocrystals, avoiding their aggregation and growth.

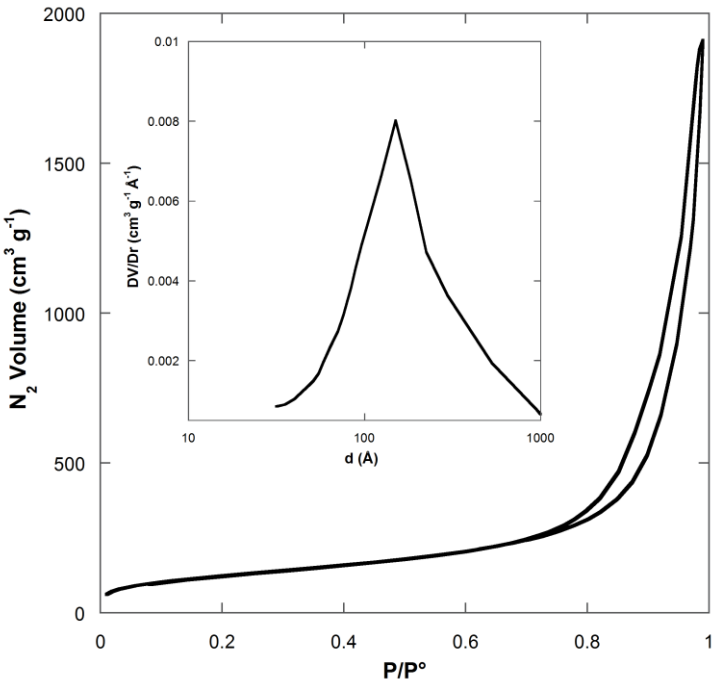

Figure S3. N_2 physisorption isotherms at 77 K of the AERO_$NiCo_2O_4$ sample and corresponding BJH pore size distribution as derived from the desorption branch (inset).

XANES

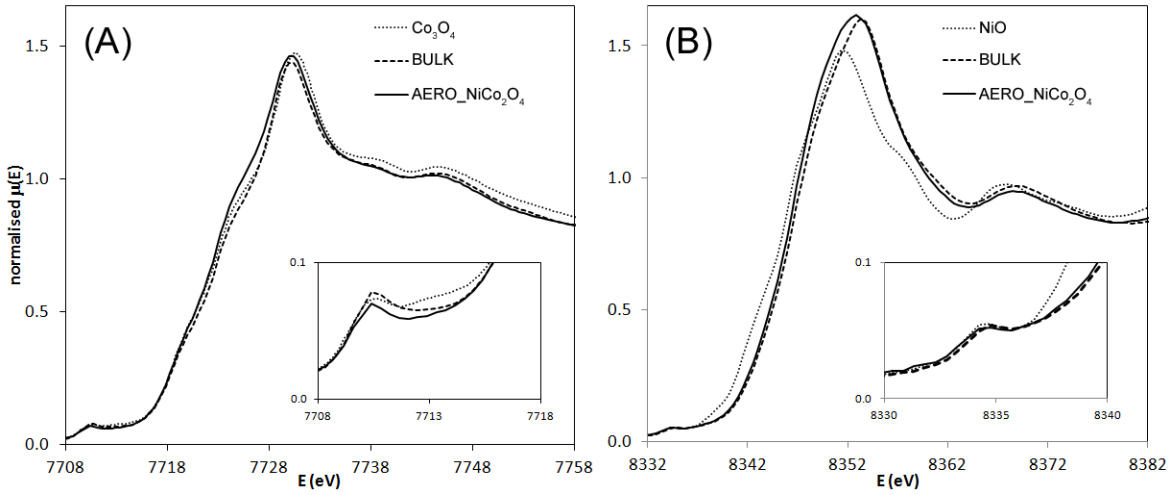

Figure S4. XANES spectra at the Co K-edge (A) and Ni K-edge (B) for Co_3O_4 (A), NiO (B), compared to AERO_$NiCo_2O_4$ and BULK

It is well known that the main absorption edge position shifts to higher energy as the oxidation state of the excited atom increases (see ref. 30). A commonly used quantitative criteria used for edge position is referred to as the "half height" position, *i.e.* the energy at which the normalized μ(E) has a value of 0.5. The oxidation states of Co and Ni in the AERO_$NiCo_2O_4$ and BULK samples have been estimated by comparison to reference compounds of Co_3O_4 for Co and NiO for Ni. This involves determining the increase in the energy of the half height position of the main absorption edge, and converting this to a change in the value of oxidation state by using a constant of proportionality (values of constants are given below).

Figure S4A shows that the Co K-edge positions in Co_3O_4 and AERO_$NiCo_2O_4$ are the same, which is consistent with the AERO_$NiCo_2O_4$ sample having an oxidation state of Co 2.67+. There is a small but real edge shift of +0.4eV to higher energy for the BULK sample. In Supplementary Info of ref 4 an edge shift of +1.8 eV between Co^{2+} and $Co^{2.67+}$ is reported.

This is consistent with the BULK sample having an increased average oxidation state of $Co^{2.82+}$.

Figure S4B shows that the Ni K-edge positions in AERO_$NiCo_2O_4$ and BULK samples have significant edge shifts of +1.1 and +1.4 eV (respectively) compared to NiO. In ref S5 a typical edge shift of +1.7 eV per +1 change in oxidation state from Ni^{2+} to Ni^{3+} to Ni^{4+} is reported. This is consistent with the AERO_$NiCo_2O_4$ and BULK samples having average oxidation states of $Ni^{2.67+}$ and $Ni^{2.82+}$ respectively.

Figure S5 shows comparisons with XANES spectra of other standards containing Co (see Supplementary Information of Ref. 4) and Ni (see Ref. 33 and Ref. S5).

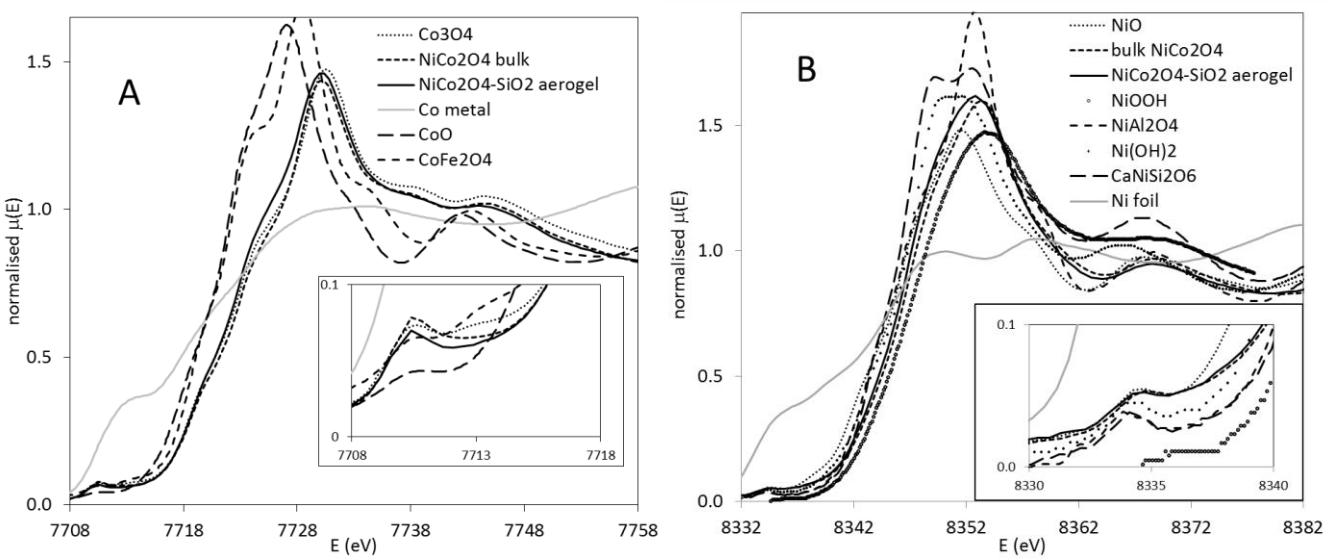

Figure S5. XANES spectra at the Co K-edge (A) and Ni K-edge (B) for a range of Co and Ni containing oxides (and hydroxides) compared to AERO_$NiCo_2O_4$ and BULK

These estimates of oxidation state are based on constants of proportionality between half height position of the main absorption edge and the value of the oxidation. These parameters have an uncertainty of 10%. There is an additional uncertainty of 5% due to the uncertainty of ±0.1 eV in the monochromator energy scale which gives an overall uncertainty of ±0.15 in the estimates of oxidation state. For this reason estimated oxidation states are reported to one decimal place in the main text of the paper.

Our interpretation of edge shift excludes some factors which may be important for other materials. These are type of ligand (which in the present case is always oxide ion), coordination, and whether specific coordination sites are regular or distorted. Coordination is not an important factor in the present case because overwhelmingly the Ni cations are located in octahedral sites, and the Co cations are evenly distributed between octahedral and tetrahedral sites. The Debye Waller factors obtained by detailed EXAFS fitting include the effects of static disorder due to distortion. Within uncertainties these Debye Waller factors show no significant differences between BULK and AERO samples. (There are no reports for Ni or Co, but a study (ref. S6) has reported the effect of geometry on "first main edge feature" of the Fe K-edge. The position was seen to vary 0.5 eV for Fe^{2+}, and 0.8 eV for Fe^{3+}, in regular vs. distorted octahedral sites, which is much smaller than the 2.4 eV shift due to change of oxidation state.)

The pre-edge peaks shown in the insets of Figure S5 have been interpreted qualitatively by comparison to those of reference oxides. Certain effects which may be important for other materials have been excluded since the type of ligand is not changing, the spin state is expected to be high spin, and the results from detailed fitting of EXAFS indicate there is no significant change in coordination or geometry, i.e. whether a specific coordination site is regular or distorted.

The Ni pre-edge peaks in BULK and AERO samples are both very similarity to NiO, consistent with octahedral coordination. The Co pre-edge peaks in BULK and AERO samples are most similar to Co_3O_4, consistent with a mixture of octahedral and tetrahedral coordination. The small differences in intensity of the sharp pre-edge peak at the Co K-edge are interpreted as being due to small differences in the proportion of Co in tetrahedral sites. We are not aware of any articles that report a detailed survey of Co pre-edge peaks at the K-edge in oxides, but this interpretation is supported by Ref. (33) on Ni pre-edge peaks at the

K-edge in oxides. That study showed that the intensity of the pre-edge peak for octahedral Ni^{2+} is in the range of 0.17 to 0.24 (normalised units) depending on degree of distortion, and increases to 0.35 for Ni^{2+} which is evenly distributed between octahedral and tetrahedral sites. Hence a slight increase in Co occupancy of tetrahedral sites is expected to have a much more significant effect on pre-edge peak intensity than a slight change in degree of distortion.

Figure S6 shows the derivatives of the spectra in Figure S4 to facilitate further comparison of the XANES spectra. These confirm that the XANES spectrum for the AERO sample has a closer similarity to Co_3O_4 than the BULK sample does.

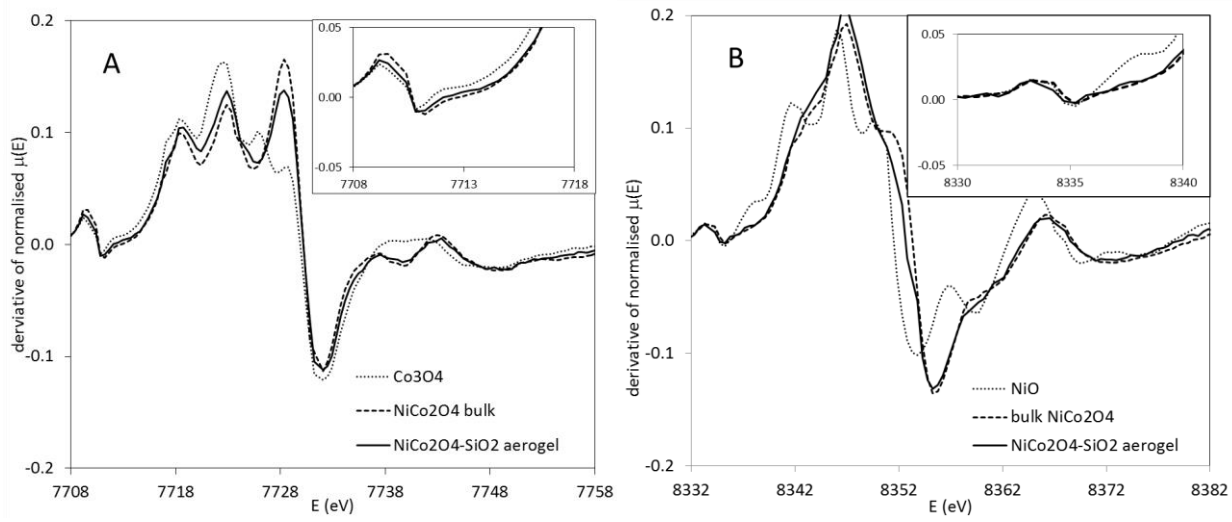

Figure S6. Derivatives of XANES spectra at the Co K-edge (A) and Ni K-edge (B) for Co_3O_4 (A), NiO (B), compared to AERO_$NiCo_2O_4$ and BULK

References

(S1) F. de Groot, G. Vanko, P. Glatzel, *J. Phys.: Condens. Matter*, 2009, **21**, 104207.

(S2) S. Brunauer, P.H. Emmet, E. Teller, *J. Am. Chem. Soc.*, 1938, **60**, 309.

(S3) P. Barret, L.G. Joyner, P.P. Halenda, *J. Am. Chem. Soc.*, 1951, **73**, 373.

(S4) F. Rouquerol, J. Rouquerol, K. Sing, *Adsorption by Powders and Porous Solids: Principles, Methodology and Applications*; Academic Press, London, 1999.

(S5) A. N. Mansour, C. A. Melendres, *J. Phys. Chem. A* 1998, **102**, 65.

(S6) G.A. Waychunas, M.J. Apted, G.E. Brown, *Phys. Chem. Minerals*, 1983, **10**, 1.